Origin of valence and core excitations in $LiFePO_4$ and $FePO_4$

2010 J. Phys.: Condens. Matter 22 275501

(http://iopscience.iop.org/0953-8984/22/27/275501)

J. Phys.: Condens. Matter **22** (2010) 275501 (8pp) doi:10.1088/0953-8984/22/27/275501

Origin of valence and core excitations in $LiFePO_4$ and $FePO_4$

M K Kinyanjui[1,2,4], P Axmann[2], M Wohlfahrt-Mehrens[2], P Moreau[3], F Boucher[3] and U Kaiser[1]

[1] University of Ulm, Albert Einstein Allee 11, 89081 Ulm, Germany
[2] Centre for Solar Energy and Hydrogen Research, Helmholtzstraße 8, 89081 Ulm, Germany
[3] Institut des Matériaux Jean Rouxel (IMN), Université de Nantes, CNRS, 2 rue de la Houssinière, BP 32229, 44322 Nantes cedex 3, France

E-mail: michael.kinyanjui@uni-ulm.de

Received 8 April 2010, in final form 19 May 2010
Published 14 June 2010
Online at stacks.iop.org/JPhysCM/22/275501

Abstract
Electronic structures of $LiFePO_4$ and $FePO_4$ have been investigated using valence and core electron energy loss spectroscopy (EELS) supported by *ab initio* calculations. Valence electron energy loss spectra of $FePO_4$ are characterized by interband transitions found between 0 and 20 eV, which are not observed in $LiFePO_4$. Spectra are fully analysed using band structure calculations and calculated dielectric functions. In particular, we show that interband transitions observed in $FePO_4$ spectra originate from the states at the top of the valence band, which have mainly oxygen p character. From core-loss EELS, it is observed that the O-K edge in $FePO_4$ has a pre-edge peak below the threshold of the main O-K edge. This pre-edge peak is not observed in the O-K spectra of $LiFePO_4$. The position of the pre-edge peak is determined by a charge transfer process, which shifts the position of the iron 3d bands with respect to the conduction band. The intensity of the pre-edge peak is also determined by the changes in the hybridization of iron 3d and oxygen states as a result of extraction of lithium ions from the $LiFePO_4$ lattice. We show that the extraction of lithium ions from $LiFePO_4$ results in large changes in the electronic structure, such that $FePO_4$ can be considered to be a charge transfer insulator while $LiFePO_4$ is a typical Mott–Hubbard insulator.

1. Introduction

In its application as a cathode material for Li ion batteries, $LiFePO_4$ shows good thermal stability, high energy density and low production costs. However, its wider application is still limited by poor electronic conductivity [1]. This has led to intensive efforts to try and understand the electronic structure of $LiFePO_4$ and how it changes with extraction (delithiation) and insertion (lithiation) of lithium (Li) ions into the lattice [2–9]. When Li ions are extracted from the lattice, charge imbalance is created within the lattice, which must be compensated either through the creation of ionic vacancies or transfer of charge carriers between ions. The charge-compensation process therefore becomes one of the driving forces behind the movement of charge within the lattice. A simplified picture of this process holds that the extraction of Li atoms from the lattice results in the Fe ion changing its oxidation state from Fe^{+II} to Fe^{+III}. It is assumed that the change in the oxidation state is directly linked to a charge modification of Fe ion (from Fe^{2+} in $LiFePO_4$ to Fe^{3+} in $FePO_4$) excluding oxygen atoms. It has long been shown in sulfur and oxygen compounds [10, 11] that this view of the charge process is oversimplified. In these studies it was shown that the oxygen atoms do indeed participate in the charge-compensation process. However, the extent to which oxygen atoms influence the process is highly dependent on the electronic structure of the compound under study. This is especially true in the case of materials which show magnetic ordering. Such a determination is still clearly necessary for $LiFePO_4$.

Experimentally, the electronic structure of $LiFePO_4$ has been studied using spectroscopic methods which include electron energy loss spectroscopy (EELS) [2–5], x-ray absorption spectroscopy [6], resonant inelastic x-ray scattering

[4] Author to whom any correspondence should be addressed.

(RIXS) [7], and Mossbauer spectroscopy [8]. In EELS, most of the studies on $LiFePO_4$ have concentrated on investigating various ionization edges rising from core–shell excitations [2, 3]. Very few papers have been devoted to studying the valence–conduction band excitations [4, 5]. This is mainly due to the difficulties encountered in interpreting valence electron energy loss spectra (VEELS). The VEELS spectrum is characterized by a number of different excitations and features that have to be taken into account before an interpretation of the spectra can be made. These excitations include plasmons, interband transitions, intra-band transitions, excitons, and relativistic losses [12–17]. In this paper we therefore go a step further than the previous investigations by studying both core–shell and valence band excitations in the EELS spectra of $LiFePO_4$ and $FePO_4$. We give a more detailed analysis of the observed valence band to conduction band excitations with the help of theoretical spectra and band structure calculations. Following a major reorganization of the electronic structure partly due the electronic onsite repulsion and local magnetic moment of Fe ions, we show that Fe–O distances, hence the covalence of the bonds, are strongly modified. The respective roles of oxygen and iron are thus demonstrated and evaluated in $LiFePO_4$.

2. Theoretical and calculation details

In EELS the fraction of incident electrons with primary energy E_0 scattered into a solid angle $\mathrm{d}\Omega$ and energy range $\mathrm{d}E$ is known as the partial differential cross section and is given by [13]

$$\frac{\mathrm{d}^2\sigma}{\mathrm{d}\Omega\,\mathrm{d}E} = \frac{1}{(\pi e a_0)^2}\frac{1}{q^2}\,\mathrm{Im}\left\{-\frac{1}{\varepsilon(q,\omega)}\right\} \tag{1}$$

where q is the momentum transfer, a_0 is the Bohr radius, and e is the charge of the electron. The function $\mathrm{Im}\{\frac{-1}{\varepsilon(q,\omega)}\}$ is known as the energy loss function and is given by [14, 15]

$$\mathrm{Im}\left\{\frac{-1}{\varepsilon(q,\omega)}\right\} = \frac{\varepsilon_2(q,\omega)}{(\varepsilon_1^2(q,\omega)+\varepsilon_2^2(q,\omega))} \tag{2}$$

where $\varepsilon(q,\omega) = \varepsilon_1 + \mathrm{i}\varepsilon_2$ is the dielectric function with ε_1 and ε_2 being the real and imaginary parts of the dielectric function respectively. An EELS spectrum can be calculated from the electronic wavefunctions and energies which are obtained by solving Kohn–Sham equations in the density functional approach (DFT) [4, 18]. In this case, the imaginary part of the dielectric tensor, ε_2 is obtained as

$$\varepsilon_2^{ij}(\omega) = \frac{4\pi^2 e^2}{m^2\left(\omega - \frac{\Delta C}{\hbar}\right)^2}\sum_{v,c}\int_{\mathrm{BZ}}\frac{2\mathrm{d}k}{(2\pi)^3} \times |\langle v_k|p_j|c_k\rangle||\langle c_k|p_i|v_k\rangle|\delta(E_{ck}+\Delta C - E_{vk} - \hbar\omega) \tag{3}$$

where $|c_k\rangle$ and $|v_k\rangle$ can be approximated by the Kohn–Sham orbitals with the wavevector $\mathbf{k}$ for the conduction and valence bands, respectively. The corresponding band energies are E_{ck} and E_{vk} respectively. The value of the scissor operator is given by ΔC, ω is the frequency, e the electron charge, m the free electron mass, and p_α the momentum operator [18]. The real part of the dielectric function ε_1 and energy loss function are then derived from ε_2 using the Kramers–Kronig transformation.

Electronic structures of the $LiFePO_4$ and $FePO_4$ were obtained by solving Kohn–Sham (KS) equations [19], within the full potential linearized augmented plane wave (FLAPW) approximation as implemented in the WIEN2k code [20]. The dielectric tensor was calculated using the Optic package included in the WIEN2k code [21]. Crystal parameters for $LiFePO_4$ and $FePO_4$ were obtained from the literature [8, 22]. We used muffin tin radii of 1.36 au, 1.46 au, 1.97 au and 2.09 au, for O, P, Li and Fe atoms respectively. The parameter $R_{\mathrm{MT}^*}K_{\max}$ was set to 7, where R_{MT} is the smallest atomic sphere radius in the unit cell and $K_{\max}$ is the magnitude of the largest K vector. The number of k-points in the irreducible part of the Brillouin zone (IBZ) was 74 and 64 for $LiFePO_4$ and $FePO_4$, respectively. In order to treat the effects of local Coulomb interactions due to Fe 3d electrons, the GGA + U method was used, as given in literature [23]. The value of the effective Coulomb parameter was set to $U_{\mathrm{eff}} = 4$ eV for both sets of calculations. Anti-ferromagnetic (AFM) supercells were used for both $LiFePO_4$ and $FePO_4$ calculations with an AFM ordering along the b axis. In the calculation of the dielectric tensor, denser meshes of 286 k-points and 195 k-points in the IBZ were used for $LiFePO_4$ and $FePO_4$, respectively. The values of scissors operators used in the optical calculations were 1 eV and 2 eV for $FePO_4$ and $LiFePO_4$, respectively [4]. $LiFePO_4$ and $FePO_4$ have an orthorhombic crystal structure and therefore the energy loss function and the dielectric function are anisotropic. However, since the experimental EELS spectra were obtained from a polycrystalline sample, the measured energy loss functions are in fact averaged over all crystal directions. Therefore, in order to compare the calculated energy loss function with experimental data, we have thus calculated the average of the diagonal elements of the dielectric tensor.

3. Experimental details

In this paper lithiated ($LiFePO_4$) and delithiated ($FePO_4$) powder samples were investigated. The lithiated and delithiated samples were prepared using the recipes given in literature [24, 25]. The state of delithiation was determined from chemical analysis and confirmed by x-ray diffraction using Rietveld refinement. For EELS measurements, samples were crushed in a mortar with acetone and then transferred to a holey carbon grid for investigations. EELS spectra were acquired using a Gatan-Tridiem spectrometer attached to a Titan 80–300 kV transmission electron microscope (TEM) and operating at 80 kV. At this operating voltage the energy resolution was determined to be 0.60 eV from the full width at half width maximum (FWHM) of the zero loss peak. Acquiring EELS at this low voltage has also an advantage of minimizing the effects from Cherenkov radiation on the EELS spectra. According to Stöger-Pollach [16], Cherenkov losses cause extra peaks to be observed in the band-gap and interband region. For Cherenkov losses to be observed the following

condition has to be fulfilled, $v > c/n$, where v is the velocity of the electron at a given accelerating voltage, c is the speed of light, and n is the refractive index. At an accelerating voltage of 80 kV v is $\approx 1.51 \times 10^8$ m s^{-1}. As a result of anisotropy the refractive index of $LiFePO_4$ is within the 1.66–1.7 range [26]. The conditions for Cherenkov losses are therefore not fulfilled in this case since $v < c/n$. Lowering the acceleration voltage also minimizes the amount of beam damage that is done to the sample by the electron beam. At higher acceleration voltage, delithiation and radiolysis are observed on $LiFePO_4$ and $FePO_4$, respectively. Short exposure times in the order of 1–2 s were used during the acquisition of the low loss spectrum. The zero loss peak (ZLP) was subtracted from the low loss spectra by deconvolution of the acquired spectra with a ZLP acquired separately from the vacuum. The spectra were corrected for multiple scattering by using the Fourier-log deconvolution method. For the O-K edge the acquisition time was 10 s. The background contribution at the O-K edge was subtracted after fitting of the background using a power law AE^{-r}, with E being the energy loss, and A and r being constants. In order to remove the effects of the multiple scattering, core-loss spectra were deconvoluted with the low loss spectrum using the Fourier-ratio deconvolution method. The details on the Fourier-log and Fourier-ratio deconvolution techniques are described in literature [27].

4. Results and discussion

4.1. Valence electron energy loss spectra

In figure 1, experimental $LiFePO_4$ and $FePO_4$ energy loss functions are presented for the energy region 0–40 eV. Spectrum features are grouped into several energy regions, labelled (i)–(iv). Energy region (i) ranges between 0 and 10 eV, region (ii) between 10 and 20 eV, region (iii) from 20 to 30 eV, and energy region (iv) is found above 30 eV. In the spectrum of $FePO_4$ (plotted with the dotted line in figure 1) there is a strong peak in the energy range (i) after the onset of absorption. In the spectrum of $LiFePO_4$ this is replaced by a small shoulder at this energy range but some of us have shown that this shoulder disappears in certain experimental conditions [4]. The $FePO_4$ spectrum is also characterized by broad shoulders in the energy region between 10 and 20 eV. A common feature between both spectra is a prominent peak at about 23 ± 0.1 eV which is found in the energy range (iii). The position of this peak does not seem to change between the two phases. Similarly, both phases show a peak at the high energy side peak in region (iv). From the experimental spectra it can be observed that the most important difference between the two spectra is in energy regions (i) and (ii) between 0 and 20 eV, in which peaks can be clearly identified in the case of $FePO_4$, whereas they are missing or much less pronounced in $LiFePO_4$ VEELS spectra. In order to interpret the differences in $LiFePO_4$ and $FePO_4$ spectra, the questions to answer are: Are the observed peaks due to plasmon excitations or interband transitions? Which bands are involved in the interband transitions? What is the main character of the interband transitions and what do they say about the delithiation process in $LiFePO_4$? The remaining part will mostly concentrate on trying to answer these questions. Analysis of the calculated dielectric functions is used for this purpose.

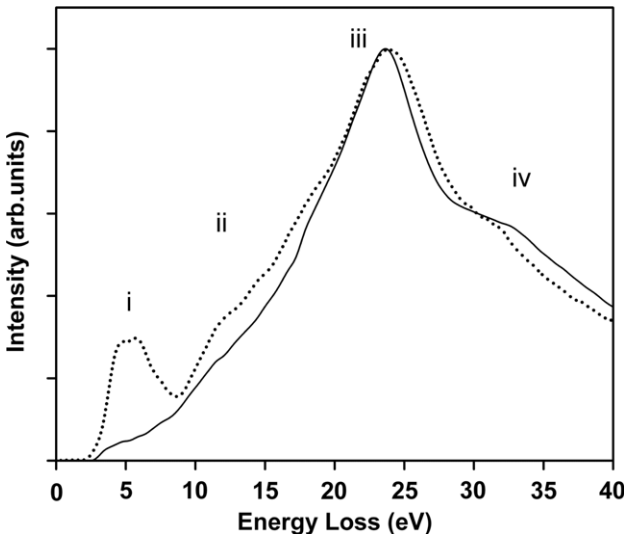

Figure 1. Experimental energy loss function (ELF) for $LiFePO_4$, (full curve) and $FePO_4$ (dotted curve). The spectrum is divided into four energy regions which have been labelled as (i)–(iv).

4.1.1. Nature of the observed peaks. The nature of the observed peaks is best obtained by studying the behaviour of the dielectric function at this energy range. Figure 2(a) shows the calculated energy loss function (black line), ε_1 (filled circles), and ε_2 (dotted line) for $LiFePO_4$. The energy loss function is mainly featureless in the low energy region below 20 eV. The most prominent peak in the energy loss function is observed at 25 eV. On the ε_2 curve, the region between 3 and 20 eV shows a strong absorption peak after which the ε_2 curve decreases steadily at higher energies. As the ε_2 curve decreases toward zero, the ε_1 curve crosses the energy axis with a positive slope just before 25 eV. The condition for plasmon excitation is thus fulfilled. This condition can be deduced from (2), where the intensity of the most prominent peak in the energy loss function should appear when $\varepsilon_1 \rightarrow 0$ and ε_2 is small [17]. Figure 2(b) shows the calculated energy loss function (black line), ε_1 (filled circles), and ε_2 (dotted line) for $FePO_4$. As was observed in the experiment (see figure 1), the calculated energy loss function and ε_2 in $FePO_4$ show features in the 0–20 eV range which are not observed in $LiFePO_4$. On the ε_2 curve, a strong absorption between 3 and 8 eV is observed. A second absorption region is then calculated between 10 and 20 eV. As for $LiFePO_4$, the ε_1 curve just crosses the energy axis with a positive slope around 24 eV which is responsible for the $FePO_4$ plasmon peak. The nature of the peak in region (iii) is thus plasmonic in both phases. The position of the calculated plasmon peak is thus overestimated by about 1–2 eV in the theoretical calculations. For both compounds, ε_2 curves show strong absorption peaks in the region 0–20 eV while ε_1 values in this range are not zero. This demonstrates that features observed in regions (i) and (ii) are due to interband transitions. After identifying the nature of the observed energy

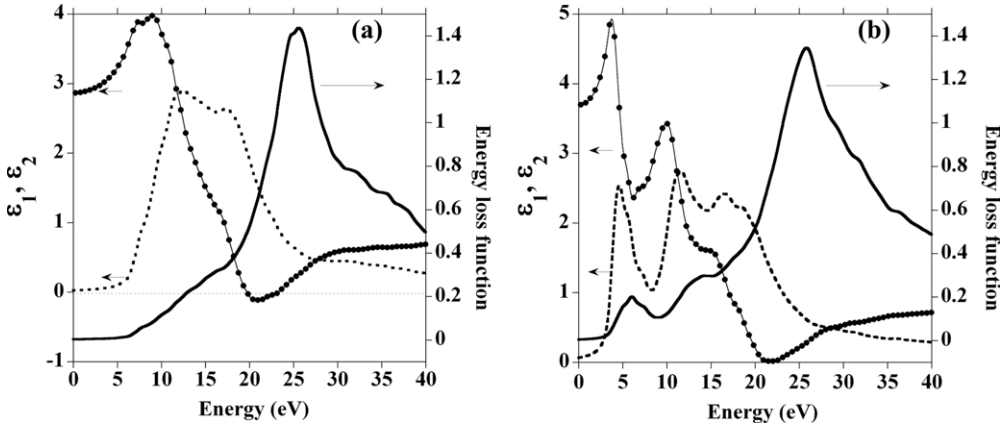

Figure 2. Calculated energy loss function (black line), imaginary (ε_2) (dotted line) and real (ε_1) (filled circles) parts of the dielectric function for (a) $LiFePO_4$ and (b) $FePO_4$. Scissor operators of 2 eV and 1 eV have been included for $LiFePO_4$ and $FePO_4$ respectively.

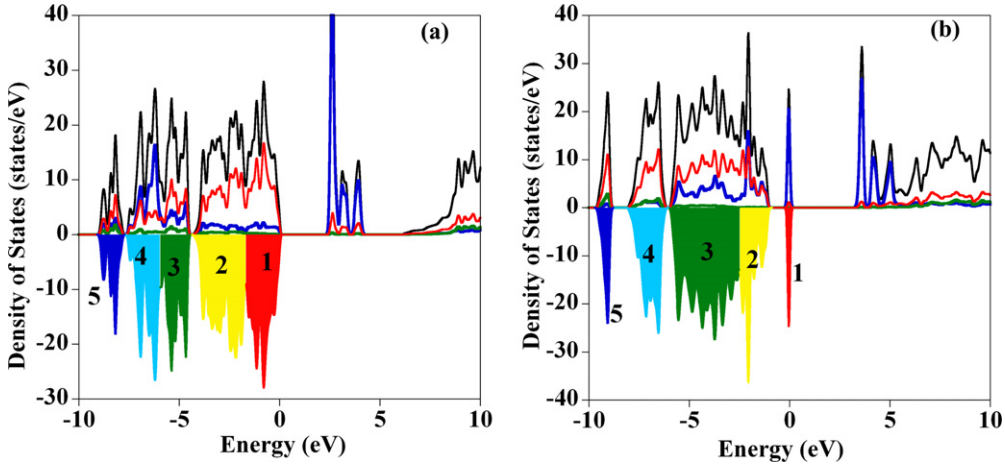

Figure 3. (a) Total density of states (spin up + spin down) (black line) for (a) $FePO_4$ and (b) $LiFePO_4$ along with partial DOS for oxygen (red line), iron (blue line) and phosphorus (green line). The different coloured regions (labelled 1–5) show the occupied density of states with a reversed axis for convenience. The Fermi level corresponds to 0 eV.

loss function features, the next task is to find out the origin and character of interband transitions found in this energy range.

4.1.2. Origin and character of the observed interband transitions. In order to investigate the origin and nature of the peaks in the energy region 0–20 eV, we use the same approach as that used by Moreau *et al*, where a theoretical dielectric function is used to interpret experimental observations [28]. In $LiFePO_4$ and $FePO_4$ electronic structures, it is particularly convenient to study separately various contributions to the total interband transitions (ε_2). The valence band was thus divided into the five energy regions for $FePO_4$ which are shown as colour filled curves (labelled 1–5, in figure 3(a)). The partial density of states for iron, oxygen and phosphorous are shown by the blue, red and green curves respectively. In a simple ionic picture with the valence states: O^{-II}, P^{V}, Fe^{+III}, one would expect fully occupied 2s and 2p oxygen bands, partially filled iron d states and empty 3s and 3p phosphorus levels. The partial density of states actually shows that this valence band is mainly oxygen in character with some iron mixing and phosphorus contributions as a result of covalent interactions. The bottom of the valence band (−9/−4 eV) originates from the bonding states of the sub unit PO_4 which can be found in numerous electronic structures of similar compounds [29]. The DOS associated with these PO_4 units constitute well separated a_1 and t_2 levels as a result of the tetrahedral symmetry (dark blue and green DOS coloured regions) [30]. In $FePO_4$, Fe d levels appear in this energy region (light blue colour DOS in figure 3(a), (region #4)). These levels make up the lower Hubbard band (LHB) whereas the upper Hubbard band (UHB) is found 2–4 eV above the Fermi level (E_F) in the conduction band. From this analysis it can seen that $FePO_4$ belongs to the charge transfer insulator type. The energy levels above 5 eV have an oxygen character due to the highly covalent antibonding interactions between the oxygen 2p states with 3s and 3p phosphorus and iron 4s states. Partial ε_2 curves resulting from interband transitions from each coloured region in figure 3(a) to the conduction band are presented in figure 4(a). All contributions show the same features: a well defined first peak is followed by another peak 7 eV higher in energy (at 3 and 10 eV for the red curve (triangles) for example). Both peaks are very much separated from each

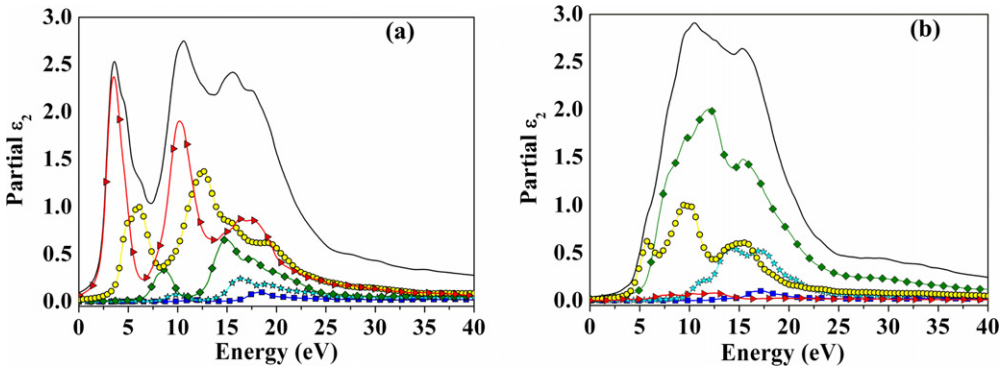

Figure 4. Calculated ε_2 curve (black line) and partial ε_2 curves (coloured lines) for (a) $FePO_4$ and (b) $LiFePO_4$ showing the interband transitions between coloured valence regions to the conduction band (CB). The partial ε_2 curves have been calculated from the coloured regions in figures 3(a) and (b) for $FePO_4$ and $LiFePO_4$ respectively. The colour code is the same as the one used in figure 3. The dark blue curve (filled squares) represents interband transitions coming from region #5, the light blue curve (stars) comes from region #4; the green curve (diamonds) is for region #3, the yellow curve (circles) corresponds to region #2 and the last red curve (triangles) account for region #1.

other. This shape in fact mimics the shape of the conduction band where the levels created by the UHB are well separated from higher energy levels (above 7 eV, in figure 3(a)). The progressive decrease of global intensity (figure 4(a), from red curve (triangles) to dark blue curve (squares)) originates from the lower valence band-conduction band oscillator strengths as the energy separation between initial and final states increases (see (3)). Another consequence of the energy dependence of the oscillator strength is that the first peak intensity decreases with respect to higher energy peaks (from the red to the dark blue curves, figure 4(a)). Compared to the dark blue region (region #5, figure 3(a)), the top of the valence band (region #1 (red) in figure 3(a)) is proportionally closer to the bottom of the conduction band ($\Delta E_1 \approx 3$ eV) than to the oxygen levels above 5 eV ($\Delta E_2 \approx 10$ eV). In the case of the dark blue curve, values are indeed $\Delta E_1 \approx 11$ eV and $\Delta E_2 \approx 18$ eV, respectively.

Intermediate valence band energy regions lead to intermediate situations with the ratio of the first peak intensity to the second one decreasing slowly. It is interesting to notice at this point that the shape of the dark blue partial ε_2 is in fact very similar to the oxygen K edge spectrum that will be discussed in next section. This proves that transitions responsible for the shape of ε_2 have a dominant oxygen character. The same kind of decomposition of the valence band is presented in figures 3(b) and 4(b) for $LiFePO_4$. The Fe ion in $LiFePO_4$ is divalent and this means that $LiFePO_4$ has an extra electron to accommodate. Therefore an additional d band is filled (−0.5/0 eV) and stabilized at a much lower energy compared to the main d levels between 3 and 6 eV (see figure 3(b)). The LHB is in this case situated at the top of the valence band (regions #1 (red) and #2 (yellow)). $LiFePO_4$ is thus close to a typical Mott insulator. Since they are not modified by a strong contribution from the Fe d levels, the levels between −10 and −6 eV present the typical a_1, t_2 shape for PO_4 tetrahedrons [30]. The partial ε_2 presents a similar shape for various starting energy regions in the valence band: a small peak or shoulder is situated in front of a very broad peak ($\Delta E_1 \approx 6$ eV and $\Delta E_2 \approx 9$ eV for the yellow curve for example). Once more, this shape essentially results from the shape of the conduction band, where the main d levels (3–5.5 eV, figure 3(b)) are very close to the other empty levels (5 eV upwards). The situation is thus very different from $FePO_4$ (compare figure 3(b) with (a)). This explains why, after adding up all partial contributions, the total ε_2 is almost featureless in the case of $LiFePO_4$ (hence the characteristic energy loss function). The d bands around E_F in fact represent only 1 electron per iron and contribute very marginally to the total ε_2 intensity. They might be responsible for the small intensity observed below 6 eV in the EELS spectrum (figure 1).

4.2. O-K edge

In the dipole approximation, which is a valid approximation for the present EELS spectra obtained at small values of momentum transfer, the O-K edge corresponds to the electronic transition from the oxygen 1s core level to unoccupied states having oxygen p character. In a purely ionic picture the divalent oxygen ion has an electronic configuration $1s^2 2s^2 2p^6$ and as such the 1s to 2p transition should not be observed. Only contributions arising from transition towards oxygen 3p states would exist but those transitions, usually observed from 15 eV above the threshold, are not very useful for the chemical bond analysis. Due to covalency, and as we have shown previously with the partial DOS analysis, states having O 2p character are found above the Fermi level. Consequently, the shape of the O-K edge can be interpreted with a band and chemical bond analysis. The intensity at the threshold is directly related to the degree of covalency of the main interactions with oxygen atoms [31–33], Fe–O and P–O in the present case.

In figure 5(a), O-K edges are presented both for $LiFePO_4$ (full line) and $FePO_4$ (dotted line). The peak features in the spectra are labelled A, B and C. The first peak which is labelled A is observed before the threshold of the main O-K edge and is hereafter referred to as the pre-edge peak. The second peak is the most prominent peak centred at 538 eV and is labelled as peak B. The third peak feature is a broad peak observed at energies above 540 eV which is labelled as peak C. Peak A appears only in $FePO_4$ while peaks B

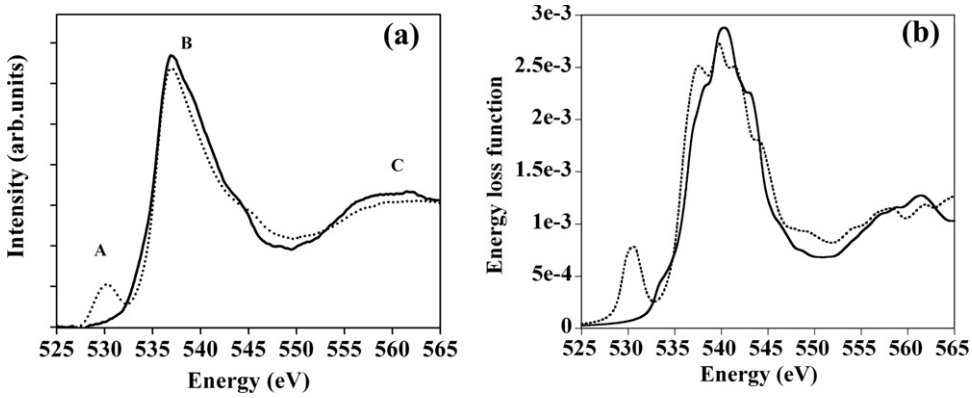

Figure 5. (a) Experimental O-K edges for $LiFePO_4$ (full line) and $FePO_4$ (dotted line). The various peaks have been marked as A, B, C respectively. Peak A is hereafter referred to as the pre-edge peak. (b) Calculated O-K edges for $LiFePO_4$ (full line) and $FePO_4$ (dotted line).

and C are observed in both $LiFePO_4$ and $FePO_4$. Usually, O-K edges are calculated using core level approaches as implemented in the Telnes/WIEN2k package. Since each unit cell contains six non-symmetry related oxygen sites, the individual contributions have to be summed in order to calculate the total O-K edge spectrum. Due to differences in energy references for the 1s level, individual spectra however have to be realigned with respect to each other before summation. This heavy procedure may be avoided in the present case using the dielectric formalism as implemented in the Optic/WIEN2k package, assuming that $\mathrm{Im}(-1/\varepsilon) \sim \varepsilon_2$ in this energy range. For this purpose, oxygen 1s states have been included into the valence by using non-conventional basis sets for the oxygen atoms. Keeping the initially obtained self consistent charge density frozen, the 1s and 2s states were described with local orbitals (LO) and standard APW + lo, respectively, and the 3s states were not considered. The energy references for the linearization were taken as the atomic 1s core state energies for the LO, and as the centre of the oxygen 2s band for the APW + lo. This specifically designed basis set was used to build the Hamiltonian matrix and hence determine the Kohn–Sham eigenvalues and wavefunctions needed for the Optic calculation. The accuracy of the present adaptation was checked by comparing the as obtained total DOS with those shown in figures 3(a) and (b). No noticeable difference could be found when considering the shape of valence and conduction bands. The loss function for the O-K edge was obtained by evaluating the imaginary part of the dielectric tensor for the transitions from the O 1s band to the conduction band and taking the average over the three Cartesian (x, y, z) directions. A broadening with a Gaussian function having a 0.6 eV full width at half maximum has been applied. For an easier comparison with experiments and because standard DFT calculations are known to not accurately reproduce the transition energy for core excitations, the calculated spectra of $FePO_4$ and $LiFePO_4$ were shifted in energy by 23 eV and 24 eV, respectively. Core–hole effects on the O-K edge were not included in these calculations. Mauchamp *et al* [34] have shown that the core–hole effects at the O-K edges are small for transition metal oxides in which the states above the Fermi level are mainly 3d states. Figure 5(b) shows the calculated O-K edges for $FePO_4$ (dotted line) and $LiFePO_4$ (full line). Our calculations reproduce the experimental features very well: a well separated pre-edge peak at 530 eV for $FePO_4$ as well as the relative intensity of this peak (peak A) compared to the main edge (peak B). The respective position of both edges is also well reproduced. The observed shift of 1 eV with respect to each other in the case of low losses is therefore also valid in the case of the O-K edge (shifts of 23 and 24 eV, respectively). The most significant differences between the calculated and experimental spectra are found in the sharp peaked feature of peak B, which is not precisely reproduced. Even if their contribution is expected to be small [34], core–hole effects could be responsible for this difference. Since the band structure calculations reproduce experimental features reasonably well, we discuss the origin of this pre-edge peak. The pre-edge peaks have been frequently observed in studies conducted on O-K edges of similar transition metal compounds, particularly in superconductors [35–37]. In these cases the pre-edge peaks were interpreted as originating from transitions from O 1s states to empty O 2p component of metal 3d hybridized with O 2p states. It is particularly interesting to note that the evolution of the O-K pre-edge in the $LiFe^{II}PO_4/Fe^{III}PO_4$ system is similar to the O-K pre-edge signature observed when doping La^{III} by Sr^{II} in $La_{2-x}Sr_xCuO_4$ [36]. According to the results obtained from calculations, La^{III}/Sr^{II} substitution creates holes at the top of the oxygen valence band which explain this pre-edge feature. However, based on the electronic structure presented in figures 3(a) and (b), the explanation for the observed pre-edge peak in the $LiFe^{II}PO_4/Fe^{III}PO_4$ system appears to be different. The evolution of the pre-edge peak in $LiFe^{II}PO_4/Fe^{III}PO_4$ has been interpreted by Sigle *et al* [5], based only on the reduction of the number of the unoccupied states due to lithium intercalation. It will be demonstrated that the actual picture is more complicated.

In transition metal compounds used in lithium ion batteries, including Li_xCoO_2 [38–40] and $Li_x[Ni_{0.3}Co_{0.3}Mn_{0.3}]O_2$ [41], it was shown that the intensity and position of the pre-edge peak gradually changes with the extraction and insertion of lithium ions. The position of the pre-edge peak is thus determined by the charge transfer, i.e. the reduction

or oxidation on the metal site, which then influences the position of the d band with respect to the conduction band. The larger the charge transfer, the closer the d band will be with respect to the conduction band. This change of the iron valence state (between Fe^{II} and Fe^{III}) can be easily observed on EELS Fe-$L_{2,3}$ edges, as previously shown for instance by Laffont *et al* [3]. On the other hand, the interpretation of the change in pre-edge intensity is not so straightforward. Considering that the cationic site geometry is not affected by the intercalation, adding/removing one lithium atom will roughly transfer/remove one electron to/from the metal d band. This will reduce/increase the number of empty d levels and consequently change the intensity of the pre-edge peak. This is not, however, the most important effect responsible for the change in intensity. As shown previously in figures 3(a) and (b), when going from $FePO_4$ to $LiFePO_4$, both phenomena, i.e. displacements of the d band and filling of one d level, are observed. An additional effect that has also to be taken into account is the change in the mixing between iron and oxygen states concerning more specifically the empty d band. The partial oxygen DOS reported for $LiFePO_4$ (figure 3(b)) is very small in this energy region when compared to $FePO_4$ (figure 3(a)). This change in the degree of hybridization between metal 3d and oxygen 2p states is a direct consequence of the increase in the energy separation between those two states and explains very well the reduction of intensity. Looking carefully at the simulated spectrum for $LiFePO_4$, the pre-edge intensity that is expected for the oxygen 2p contribution into the iron empty d band is completely hidden (around 534 eV, see figures 5(a) and (b)) into the main edge due to both its decrease in intensity and shift to higher energy. Since lithium insertion in $FePO_4$ follows a biphasic process at room temperature (mixture $LiFePO_4/FePO_4$), one observes either the pre-edge feature for the delithiated Fe^{III} compound or directly the absence of the pre-edge for the lithiated Fe^{II} material. Experiments not presented here reveal that for a metastable $Li_{0.5}FePO_4$ composition, a solid solution obtained from quenching [4], the pre-edge peak is observed at the same position as in $FePO_4$, which is the clear signature of Fe^{III}, but its intensity is reduced and only depends on the Fe^{III}/Fe^{II} ratio.

5. Conclusions

We have investigated the valence and core electron energy loss spectra in $LiFePO_4$ and $FePO_4$. Experimental results have been interpreted using *ab initio* calculations of the band structure, theoretical dielectric function and core-spectra. The valence energy loss spectra of $LiFePO_4$ and $FePO_4$ show some characteristic differences in the observed peaks. $FePO_4$ spectra show several peaks in the energy range 0–20 eV which are either missing in $LiFePO_4$ or are much less intense. Electronic calculations show that $LiFePO_4$ could be considered to be a Mott–Hubbard insulator while $FePO_4$ is a charge transfer insulator. Based on this we have shown that the first interband transition observed in $FePO_4$ VEELS spectra originates from the energy states at the top of the valence band which have mainly oxygen 2p character. The core-loss spectrum of the O-K edge in $FePO_4$ also shows a pre-edge peak that is observed before the threshold of the O-K edge. This peak is hidden in the main intensity (around 534 eV) in both theoretical and experimental $LiFePO_4$ spectra. The differences in the O-K spectra between $LiFePO_4$ and $FePO_4$ are also reproduced in calculated O-K edges. The pre-edge peak at the O-K edge is interpreted to be due to transitions from the O 1s state to the O 2p component of the Fe 3d–O 2p states in the conduction band. An alternative method to calculate the O-K edge was also presented to avoid the long procedure of core level approaches in large systems with inequivalent oxygen atoms. It is expected that similar calculations could be performed in many instances where multiple spectra of inequivalent atoms have to be added.

Acknowledgments

We would like to thank Soeren Selve, Sabine Groezinger, Bianca Anglet and Sandra Stroebele for their assistance in preparing the samples and in conducting the electrochemical measurements. We gratefully acknowledge the financial support of this work by the German Federal Ministry of Education and Research (BMBF) and German Research Foundation (DFG).

References

[1] Padhi A K, Nanjundaswamy K S and Goodenough J B 1997 *J. Electrochem. Soc.* **144** 1188
[2] Miao S, Kocher M, Rez P, Fultz B, Yazami R and Ahn C C 2007 *J. Phys. Chem.* A **111** 4242
[3] Laffont L, Delacourt C, Gibot P, Wu M Y, Kooyman P, Masquelier C and Tarascon J M 2006 *Chem. Mater.* **18** 5520
[4] Moreau P, Mauchamp V, Pailloux F and Boucher F 2009 *Appl. Phys. Lett.* **94** 123111
[5] Sigle W, Amin R, Weichert K, van Aken P A and Maier J 2009 *Electrochem. Solid-State Lett.* **12** A151
[6] Augustsson A, Zhuang G V, Butorin S M, Osorio-Guillén J M, Dong C L, Ahuja R, Chang C L, Ross P N, Nordgren J and Guo J H 2005 *J. Chem. Phys.* **123** 184717
[7] Hunt A, Ching W Y, Chiang Y M and Moewes A 2006 *Phys. Rev.* B **73** 205120
[8] Andersson A S, Kalska B, Haggstrom L and Thomas J O 2000 *Solid State Ion.* **130** 41
[9] Tang P and Holzwarth N A W 2003 *Phys. Rev.* B **68** 165107
[10] Dupin J C, Gonbeau D, Martin-Litas I, Vinatier P and Levasseur A 2001 *J. Electron. Spectrosc. Relat. Phenom.* **120** 55
[11] Wu Z Y, Ouvrard G, Lemaux S, Moreau P, Gressier P, Lemoigno F and Rouxel J 1996 *Phys. Rev. Lett.* **77** 2101
[12] Sturm K 1982 *Adv. Phys.* **31** 1
[13] Fink J, Nucker N, Pellegrin E, Romberg H, Alexander M and Knupfer M 1994 *J. Electron. Spectrosc. Relat. Phenom.* **66** 395
[14] Bell M G and Liang W Y 1976 *Adv. Phys.* **25** 53
[15] Tews W and Gründler R 1982 *Phys. Status Solidi* b **109** 255
[16] Stöger-Pollach M 2008 *Micron* **39** 1092
[17] Philipp H R and Ehrenreich H 1963 *Phys. Rev.* **129** 1550
[18] Ambrosch-Draxl C, Majewski J A, Vogl P and Leising G 1995 *Phys. Rev.* B **51** 9668
[19] Kohn W and Sham L J 1965 *Phys. Rev.* **140** A1133
[20] Blaha P, Schwarz K, Madsen G K H, Kvaniscka D and Luitz J 2001 *WIEN2k, An Augmented Plane Wave + Local Orbitals Program for Calculating Crystal Properties* Schwarz K, Techn. Universität Wien, Austria

[21] Ambrosch-Draxl C and Sofo J O 2006 *Comput. Phys. Commun.* **175** 1
[22] Streltsov V A, Belokoneva E L, Tsirelson V G and Hansen N K 1993 *Acta Crystallogr.* B **49** 147
[23] Zhou F, Kang K S, Maxisch T, Ceder G and Morgan D 2004 *Solid State Commun.* **132** 181
[24] Axmann P, Stinner C, Wohlfahrt-Mehrens M, Mauger A, Gendron F and Julien C M 2009 *Chem. Mater.* **21** 1636
[25] Arnold G, Garche J, Hemmer R, Strobele S, Vogler C and Wohlfahrt-Mehrens M 2003 *J. Power Sources* **119** 247
[26] Anthony J W, Bideaux R A, Bladh K W and Nichols M C 2000 *Handbook of Mineralogy* vol IV (Tucson, AZ: Mineral Data Publishing)
[27] Egerton R G 1986 *Electron Energy Loss Spectroscopy in the Electron Microscope* (New York: Plenum)
[28] Moreau P and Cheynet M C 2003 *Ultramicroscopy* **94** 293
[29] Launay M, Boucher F, Gressier P and Ouvrard G 2003 *J. Solid State Chem.* **176** 556
[30] Gauthier G, Jobic S, Boucher F, Macaudiere P, Huguenin D, Rouxel J and Brec R 1998 *Chem. Mater.* **10** 2341
[31] de Groot F M F, Grioni M, Fuggle J C, Ghijsen J, Sawatzky G A and Petersen H 1989 *Phys. Rev.* B **40** 5715
[32] Grunes L A, Leapman R D, Wilker C N, Hoffmann R and Kunz A B 1982 *Phys. Rev.* B **25** 7157
[33] Grioni M, Czyzyk M T, de Groot F M F, Fuggle J C and Watts B E 1989 *Phys. Rev.* B **39** 4886
[34] Mauchamp V, Jaouen M and Schattschneider P 2009 *Phys. Rev.* B **79** 235106
[35] Yuan J, Brown L M, Liang W Y, Liu R S and Edwards P P 1991 *Phys. Rev.* B **43** 8030
[36] Nücker N, Fink J, Fuggle J C, Durham P J and Temmerman W M 1988 *Phys. Rev.* B **37** 5158
[37] Kuiper P, Kruizinga G, Ghijsen J, Grioni M, Weijs P J W, de Groot F M F, Sawatzky G A, Verweij H, Feiner L F and Petersen H 1988 *Phys. Rev.* B **38** 6483
[38] Yoon W S, Kim K B, Kim M G, Lee M K, Shin H J, Lee J M, Lee J S and Yo C H 2002 *J. Phys. Chem.* B **106** 2526
[39] van Elp J, Wieland J L, Eskes H, Kuiper P, Sawatzky G A, de Groot F M F and Turner T S 1991 *Phys. Rev.* B **44** 6090
[40] Laubach S, Laubach S, Schmidt P C, Ensling D, Schmid S, Jaergermann W, Thissen A, Nikolowski K and Ehrenberg H 2009 *Phys. Chem. Chem. Phys.* **11** 3278
[41] Kim M G, Shin H J, Kim J H, Park S H and Sun Y K 2005 *J. Electrochem. Soc.* **152** A1320